Synthesis and Characterization of Peptide Grafted Porous Polymer Microstructures

Trent R. Northen,[†,‡] Daniel C. Brune,[‡] and Neal W. Woodbury*[,†,‡]

Biodesign Institute at Arizona State University and Department of Chemistry and Biochemistry, Arizona State University

Received September 20, 2005; Revised Manuscript Received January 9, 2006

A scanning laser system has been used to generate three-dimensional trimethylolpropane trimethacrylate (TRIM) cross-linked poly(2-hydroxylethyl methacrylate) polymer microstructures through azo-bis(isobutyro)nitrile (AIBN) photopolymerization using a 20 × 0.5 NA microscope objective and 365 nm laser excitation. Macropores are observed to form without the use of porogens in regions of highest light flux. This is attributed to phase separation, which results from differences in monomer reactivity and miscibility. The microstructures were aminated and then protected with the photolabile protective group 6-nitroveratryloxycarbonyl (NVOC). This made it possible to selectively modify the microstructures with the same scanning laser system that was used to fabricate them, resulting in peptide grafted three-dimensional porous microstructures. On the basis of the absorbance of the dibenzofulvene−piperidine, these structures have an amine site density of ∼0.1 nmol/feature. MALDI-TOF MS was used to characterize peptide photografted microstructures. *N*-Tris(2,4,6-trimethoxyphenyl)phosphonium (TMPP) labeling of the peptides greatly enhanced detection and allowed post-source decay sequencing of the peptides from the microstructures. The techniques described could be used to generate three-dimensional peptide grafted porous scaffolds for tissue engineering applications.

Introduction

Tissue engineering seeks to construct artificial tissues for the replacement, repair, and regeneration of tissue/organ function. One approach to tissue engineering is to use synthetic polymeric scaffolds that are grafted with peptides which support cell adhesion and subsequent cell seeding.[1] The combination of cells and polymer scaffolds has made it possible to make a number of replacement tissues including skin, bone, cartilage, and others.[2,3] To construct more complex tissues such as organs, it will be necessary to immobilize multiple cell types on scaffolds which allow for efficient transfer of gases, nutrients, and waste.[3]

Recent advances in photopolymerization have been made allowing the construction of microscale and complex nanoscale structures from photopolymers[4−8] using scanning laser systems. Kawata has shown a 3D fabrication accuracy of 150 nm using two-photon polymerization,[4] and Maruo has used oxygen quenching in conjunction with one-photon patterning to create 3D microstructures with resolution of <1 um.[5] Recently, Ober showed the construction of ethylene glycol dimethacrylate cross-linked poly(2-hydroxylethyl methacrylate) microstructures using lithography.[9]

Interfacing these advanced polymerization techniques with light-directed synthesis could enable the construction of tissue scaffolds with complex three-dimensional structures.[10] With the use of appropriate functional groups on the polymer and photocleavable blocking groups to allow optical patterning, it is possible to perform spatially defined chemical synthesis.[11] Such approaches are commonly used to construct 2D microarrays, particularly DNA chips, which have found broad application,[12−14] but the extension of optically patterned chemical modification to systems with 3D architectures is in its infancy.

Photopolymer microstructures are typically nonporous structures. To improve mass transfer through the scaffold, it would be desirable to develop macroporous structures similar to those Frechét and Svec have developed,[15,16] which have proven very useful for microanalytical systems.[17] Here, these structures are molded, and the pores are formed using high concentrations (>50%) of cosolvents known as porogens[18−20] to form porous structures inside capillary channels. Porous structures are a result of a phase separation that occurs when the growing polymer chain precipitates from the monomer/porogen solution. More recently, lithographic photopolymerization in the presence of porogens was used to form the monoliths with controlled pore sizes[21,22] and to modify their surfaces[23] within the capillary.

Recently, Luo and Shoichet[24,25] showed peptide photografting of agarose hydrogels using photolabile *S*-(2-nitrobenzyl)cysteine. Here, a bulk gel is modified by using either a UV lamp or a focused laser beam allowing immobilization of a maleimido-terminated biomolecules. This is an important step toward the construction of complex three-dimensional biomolecule modified polymer structures.

Previously,[26] we reported developments in laser micropatterning techniques for the construction of polymer microstructures. Interestingly, through an unknown mechanism, porous structures were obtained at the focal point of the laser without the use of porogenic solvents. Here, we propose a mechanism for pore formation in regions of highest light flux and describe light-directed solid-phase synthesis and grafting of peptides onto these structures. A scheme for microstructure formation and photografting is illustrated in Figure 1. This approach may allow the construction of complex porous 3D polymer scaffolds which are selectively modified with biomaterials to control cell proliferation, growth, and so forth.

* E-mail: nwoodbury@asu.edu.
† Biodesign Institute.
‡ Department of Chemistry and Biochemistry.

10.1021/bm0506952 CCC: $33.50
Published on Web 02/18/2006

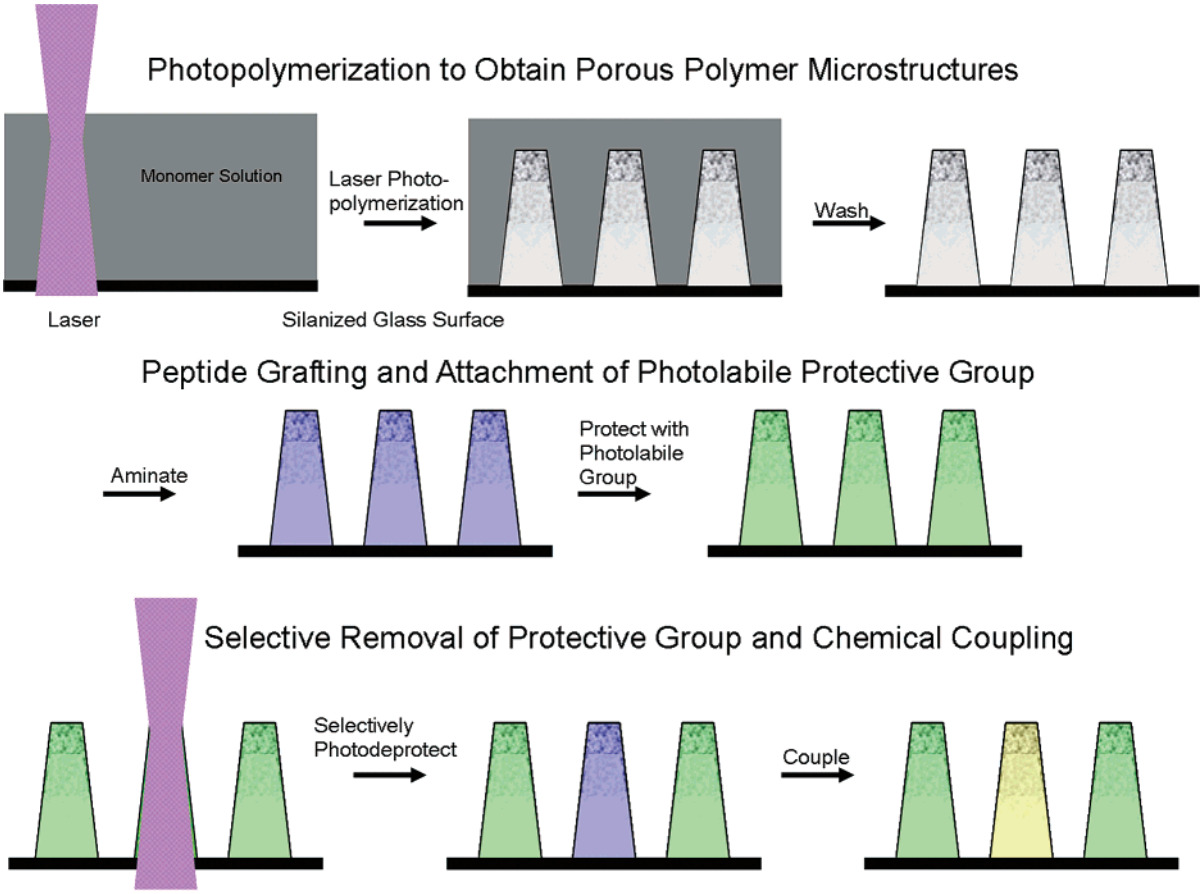

Figure 1. Cartoon illustrating synthetic approach: nonlinear laser photopolymerization to obtain porous polymer structures, surface modification of structures including addition of a photolabile protective group (green), selective removal of the protective group (blue), and spatially addressable surface modification (green). Note that large pores form selectively at the focus of the laser.

Experimental Details

A detailed description of the microstructure preparation, functionalization, and photodeprotection is reported elsewhere.[26] These methods are briefly summarized below.

Materials. Glass coverslips were from Bioptechs (Butler, PA). 6-Nitroveratryl chloroformate and 3-(trimethoxysilyl)propyl methacrylate were from Fluka GmbH (Buchs, Switzerland). Dimethylformamide (DMF) was from Applied Biosystems Inc. (Foster City, CA). 2-hydroxylethyl methacrylate (HEMA), trimethylolpropane trimethacrylate (TRIM), azo-bis(isobutyro)nitrile (AIBN), piperidine, 1,4-dioxane, semicarbazide hydrochloride, diisopropylethylamine (DIPEA), and triisopropyl silane (TIS) were purchased from Sigma-Aldrich Chemical Co. (Milwaukee, WI). 2-Propanol and ethanol (95%) were from ACROS Organics (Geel, Belgium). Acetonitrile was from Alfa Aesar (Ward Hill, MA). Methanol, hydrogen peroxide (30%), sulfuric acid, and hydrochloric acid were purchased from Mallinckrodt Inc. (Paris, KY). ACS dichloromethane (DCM) was from Burdick & Jackson (Muskegon, MI). 2-(1*H*-benzotriazole-1-yl)-1,1,3,3-tetramethyluronium hexafluorophosphate (HBTU), Fmoc−phenylalanine (Fmoc−Phe), Fmoc−leucine (Fmoc−Leu), Fmoc−tyrosine (Fmoc−Tyr), Fmoc−proline (Fmoc−Pro), Fmoc−glycine (Fmoc−Gly), and trifluoracetic acid (TFA) were from Advanced ChemTech Inc. (Louisville, KY). Fmoc-Rink linker was from NovaBiochem, a division of EMD Biosciences, Inc. (San Diego, CA), and Texas Red sulfonyl chloride was from AnaSpec Inc. (San Jose, CA). Finally, water was purified using a NANOPure ultrapure filtration system from Barnstead (Dubuque, IA). TMPP−acetic acid *N*-hydroxysuccinimide ester (TMPP−Ac−OSu−Br) was prepared following the method described by Huang et al.[27] The mass spectrometry matrixes 4-hydroxybenzylidenemalononitrile (4-OH BMN) and α-cyano-4-hydroxycinnamic acid were from Lancaster Synthesis Inc. (Windham, NH) and Aldrich Chemical Co. (Milwaukee, WI), respectively.

Equipment. An FCSII flow chamber from Bioptechs Inc. (Butler, PA) was used for all photoreactions. Patterning was performed using a mode-locked Tsunami Ti:sapphire laser pumped by a 5 W Millennia Vs diode-pumped cw laser, Spectra-Physics Inc. (Mountain View, CA), a 20 × 0.5 NA objective attached to an Eclipse TE2000-U microscope, Nikon Inc. (Japan) with a ProScan microscope stage, Prior Scientific Inc. (Rockland, MA). The laser beam was shuttered using a model 350-80 electro-optic light modulator with model 302 power supply, Conoptics Inc. (Danbury, CT), controlled by software developed in-house. A frequency doubler, U-Oplaz Technologies Inc. (Chatsworth, CA), was used to generate the 365 nm light. Images were obtained using excitation from a 100 W Hg arc lamp, Oriel Scientific (Stratford, CT) and a 560/40 (center wavelength/bandwidth) excitation filter, and fluorescence was collected through a D630/60 emission filter, both from Chroma Technologies Corp. (Rockingham, VT) by a SenSys 1400 CCD camera from Roper Scientific (Tuscon, AZ). Absorbance measurements were performed using a Cary 50 UV−vis spectrophotometer, Varian Inc., (Palo Alto, CA). Scanning electron microscopy (SEM) was performed using a XL30ESEM environmental SEM, FEI Co. (Hillsboro, OR) on a sample coated with 3.5 nm palladium/gold. Mass spectrometry was performed using a Voyager-DE STR MALDI-TOF mass spectrophotometer, Applied Biosystems Inc. (Foster City, CA).

Surface Functionalization. Glass cover slides were cleaned using a modification of methods reported in previous work.[26]

Fabrication of Polymer Structures. In general, solutions composed of 43 mol % HEMA in TRIM and 0.5−1% in AIBN were prepared and placed in the optical chamber and irradiated at room temperature with 4 mW of 365 nm light for 2 s per feature. A 20× objective was used to focus the light 400 μm above the surface of the cover slip. Arrays with features spaced 600 μm apart were constructed. Excess monomer was drained, and sample was washed with methanol and DMF.

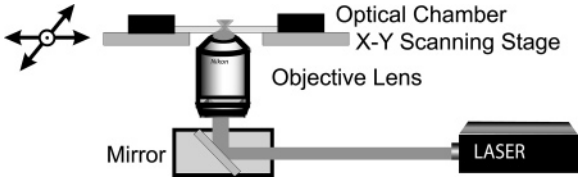

Figure 2. Scanning laser system used to make the polymer microstructures.

Amination of Microstructures. Either 63 μmoles of Fmoc-Rink (33.7 mg) or Fmoc−Gly (18.6 mg) was coupled to the photopolymer hydroxyl group using 22.5 mg (59 μmol, 0.94 equiv) HBTU and 11.5 μL (66 μmol, 1.5 equiv) DIPEA in 600 μL DMF for 3 min. Fmoc-Rink or Fmoc−Gly, DIPEA, and DMF were combined and reacted for 3 min, and this was then added to the chamber and reacted with mixing at 50 °C for 30 min. The structures were then rinsed with DMF and the Fmoc removed with 20% piperidine in DMF for 10 min. The number of amino groups coupled was determined by monitoring the absorbance at 301 nm of the Fmoc−piperidine adduct released (ϵ = 7800 $M^{-1} \times cm^{-1}$). Typical polymer amine site densities were estimated to be on the order of 0.1 nmol/feature.

Peptide Synthesis. In general, coupling steps were performed by reacting 63 μmol of Fmoc−amino acid, 22.5 mg (59 μmol, 0.94 equiv) HBTU, and 11.5 μL (66 μmol, 1.5 equiv) DIPEA in 600 μL DMF for 3 min, then adding to the microstructures and reacting at 50 °C for 1 h. The surface was rinsed with DMF until the absorbance at 300 nm was <0.1, washed twice for 10 min with 20% piperidine in DMF, and then washed with DMF to remove the piperidine.

Peptide Coupling. Peptides were prepared using Fmoc chemistry on a MilliGen/Biosearch 9050 peptide synthesizer and coupled to the microstructures using the same method described above.

Coupling NVOC to Aminated Microstructures. A solution of 19 mg NVOC in 40 μL DIPEA and 600 μL DMF was reacted with the aminated polymer microstructures by mixing for 30 min at 50 °C.

Laser Cleavage of NVOC. The same laser beam used to make the microstructures was used to selectively remove the NVOC. The beam was attenuated as needed. The sample was immersed in dioxane or 60 mM semicarbazide HCl in DMF or acetonitrile with 3% DIPEA.

Labeling Microstructures. Texas Red-SC in DMF at 1 mg/mL was added to the microstructures and reacted for 2 h at room temperature, after which the microstructures were washed with DMF to remove unreacted dye. TMPP−Ac−OSu−Br was prepared following the method described by Huang et al.[27] and was coupled to the peptide grafted microstrostructures by reacting a solution of 0.5 mg TMPP−Ac−OSu−Br, 20 μL DIPEA, and 480 μL DMF with the microstructures for 1 h at 35 °C.

Results and Discussion

Polymer Microstructures. HEMA was selected as the primary monomer because it is very polar, nontoxic, and biocompatible.[9,28] TRIM was selected as the cross-linker because of its lack of fluorescence, which may interfere with fluorescent imaging of materials bound to the structure, and the many examples of its use in forming porous structures.[18,19] Polymer structures were obtained via the photopolymerization of HEMA and TRIM with AIBN as reported elsewhere.[26] The setup for the scanning laser system is illustrated in Figure 2. Briefly, the light is focused using a microscope objective and modulated with an optical shutter, and the sample is moved within the stationary laser beam using an $x-y$ stage. AIBN forms free radicals upon exposure to UV light; these can initiate polymerization. However, if oxygen is present, it can consume the radicals, inhibiting the photopolymerization. Since the light flux is highest within the focused laser beam, the microstructures take the shape of the laser beam because of rapid consumption of oxygen quenching with the probe volume, whereas outside of this volume, the light flux is insufficient to consume the oxygen. The microstructures are limited to the area below the focus, presumably because of scattering and light attenuation from AIBN absorption.

Scanning electron microscope images (Figure 3) revealed that the polymer structures are 400 μm tall, having an elliptical base with radii of 75 and 200 μm. This geometry gives the structures mechanical stability while maintaining a large surface-to-volume ratio for efficient mass transfer. In general, 800 microstructures were made at a time.

As seen in Figure 3, >1 μm pores are observed at the top of the microstructures, closest to the focus, where there is the highest light flux, and not elsewhere. The extremely high light flux found at the focus of the laser beam rapidly consumes the oxygen and forms a higher concentration of radicals than in regions with lower light flux. TRIM is a trimethacrylate and is incorporated into the polymer at a higher rate than HEMA, which is a monomethacryate. This presumably results in formation of a TRIM-rich polymer phase and HEMA-rich monomer phase.

In this case, pore formation is attributed to phase separation and incomplete polymerization of the monomer phase. Following photopolymerization, the remaining monomer is removed with solvent, resulting in the porous structure. The phase separation can be understood in terms of differences in the solubility parameters[29] of the polymer and monomer phases

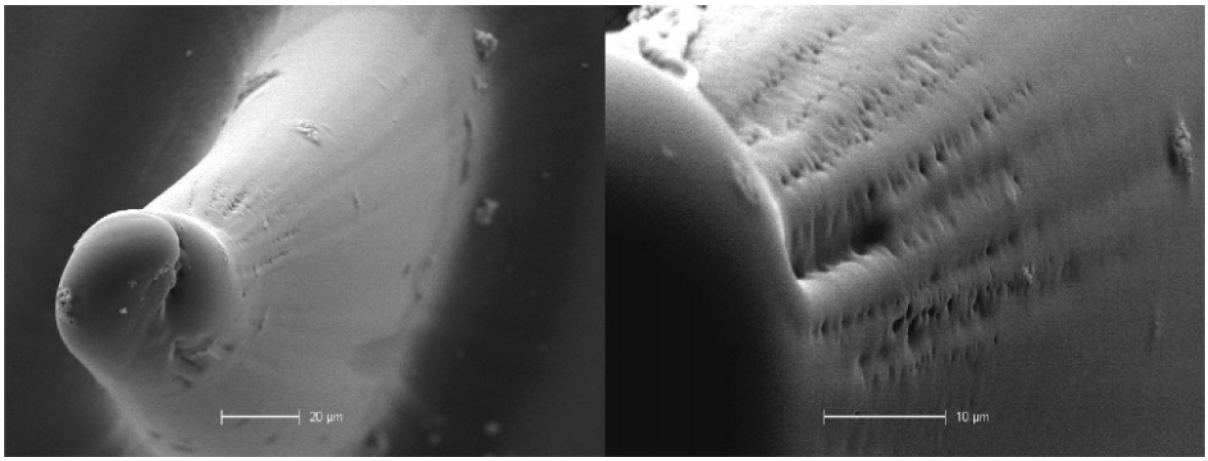

Figure 3. SEM images of TRIM/HEMA polymer microstructures on glass. The perspective is looking down at the microstructures from above: (left) one microstructure, (right) macropores below tip of microstructure.

Table 1. Hildebrand Solubility Parameter for Monomers and Polymers of Interest

material	Hildebrand solubility parameter [$MPa^{1/2}$]
HEMA[30]	23.3
TRIM[18]	18.0
polyHEMA[30]	29.7
polyTRIM[18]	18.2

within this region. Briefly, the solubility parameter is a measure of the attractive strength between molecules within a material and is very useful in understanding the phase separation process which leads to porous polymer structures. In general, a polymer will swell and/or dissolve in a diluent with a solubility parameter within a couple of megapascals$^{1/2}$. In this case, the diluent (monomer solution) has a solubility parameter of $\sim$20 $MPa^{1/2}$. However, as can be seen in Table 1, polymers of these two monomers have very different solubility parameters from the two monomers, and the TRIM-rich polymer would be expected to have decreased solubility in a HEMA-rich monomer solution. In regions with lower light flux, this phase separation is not observed, presumably because of a decreased rate of oxygen consumption, which limits the polymerization process such that sufficient HEMA is incorporated to prevent phase separation.

This ability to make large pores in some regions and not in others depending on the light flux may serve as a useful tool for the construction of scaffolds where it is desirable to have large pores that persist irrespective of solvent/environment. It may be possible to increase the pore size sufficiently to allow cell seeding and growth of cells within the structures by using less compatible monomers to cause earlier phase separation. In this case, it is likely that cell proliferation will be limited to porous regions, implying that 3D spatial control of porosity may allow for spatial control of cellular growth and proliferation.

Arrays of microstructures spaced 600 μm apart were constructed. The surface was aminated with either Fmoc−Gly for photopatterning experiments, or the acid labile Fmoc-Rink linker was used when samples were to be characterized by MALDI-MS. The number of reactive sites (using the dibenzofulvene−piperidine adduct absorption at 301 nm) was estimated to be 0.1 nmol per feature.

Light-Directed Fluorescent Dye Patterning on Microstructures. Attachment of the photolabile NVOC group to the N-terminus of the glycine grafted polymer allowed the selective removal of the protective group using the scanning laser system with the same objective and focus used to make the microstructures. It was found that upon excessive light exposure adjacent features were deprotected. Optimal exposure times were determined through the use of Texas Red-SC, an amine reactive fluorescent dye, by exposing alternating microstructures and then reacting the array with the dye. By varying the exposure time, coupling the dye, and imaging the intensity of both the illuminated and adjacent nonilluminated structures, the optimal exposure time with 4 mW of 365 nm laser light was found to be 500 ms per feature (Figure 4). The fluorescence intensity from these microstructures was clearly visible to the eye using a handheld lamp for excitation.

MALDI-MS on Peptide Grafted Microstructures. Estimates based on release of the dibenzofulvene−piperidine adduct suggested that enough reactive sites were present on the photopolymers to allow MALDI-MS characterization of materials grafted or synthesized on the microstructures. To test this, photopolymer microstructures were aminated with the TFA labile Rink amide linker, and the peptide Fmoc−Pro-Gly-Gly-Phe-Leu (Fmoc−PGGFL) was coupled to the microstructure

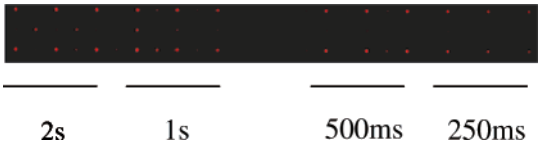

Figure 4. Optimization of exposure time using fluorescence from photopatterned Texas Red dye grafted array of microstructures deprotected using four different exposure times. All exposed features are surrounded by unexposed features to control for the effects of scattered light. Note that the same scanning laser system and focus is used to perform photopatterning as to fabricate microstructures.

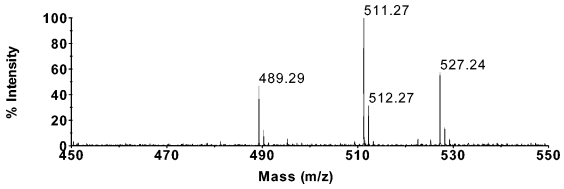

Figure 5. MALDI-MS spectrum for the cleavage of PGGFL−amide from photopolymer microstructure shows the protonated peptide at 489.29 Da (489.28 Da theoretical), the sodium adduct at 511.27 Da (511.26 Da theoretical), and the potassium adduct at 527.24 Da (527.24 Da theoretical) using a 1:10 dillution of sample and saturated solution of 4-OHBMN in 50% acetonitrile, 0.1% TFA, and Nanopure water.

surfaces. After removing the Fmoc, this linker was cleaved with TFA, and the resulting solution was concentrated and mixed with the matrix 4-OHBMN. MALDI-TOF (Figure 5) clearly shows the sodium adduct of PGGFL−amide at 511.27 Da (511.26 Da theoretical mass) to be the major ion using a 1:10 dillution in matrix solution.

MALDI-MS on an in situ Synthesized Peptide. A total of 351 polymer microstructures were prepared and functionalized with the acid labile Rink linker as before. Fmoc synthesis was used to make Phe-Leu-Phe (FLF) on all microstructures. The N-terminus was then blocked with the photolabile group NVOC. These were then deprotected in dioxane using the same scanning laser system, and Fmoc−Leu was coupled. The Fmoc group was removed, and half of the features were placed in separate Eppendorf tubes and dissolved in DCM/TFA/ TIS to cleave the Rink linker. This solution was decanted, dried, and dissolved in the 4-OHBMN solution and spotted onto the MALDI-MS sample plate at various dilutions. MALDI-MS showed a small peak corresponding to the Na^+ adduct of LFLF−amide in the leucine treatment area (576.25 Da vs 576.32 Da predicted).

Improved Ion Formation and Peptide Sequencing Using N-Terminal Modification. The group *N*-tris(2,4,6-trimethoxyphenyl)phosphonium (TMPP)[27] was used to improve ion formation and to confirm the sequence of a peptide grafted onto the polymer microstructures. In this case, Fmoc−GGFL was coupled to the Rink-derivatized microstructures. Substitution of the NVOC group for Fmoc allowed the selective light-directed attachment of TMPP. MALDI-MS from 175 microstructures resulted in the spectrum shown in Figure 6 where the major ion at 964.40 Da corresponds to the predicted TMPP−GGFL−amide Na^+ adduct (964.41 Da). Also, the correct isotopic distribution was observed. The NVOC−GGFL−amide Na^+ adduct (653.25 Da predicted) is clearly seen in both spectra, indicating that in this case the photocleavage reaction did not go to completion.

The fact that the TMPP group facilitates the observation of fragment ions[27] was used to sequence the peptide. This was done by selecting the 964.40 Da ion for postsource decay analysis, and its fragmentation pattern was used to determine the sequence of the peptide (Figure 7). The same primary ion

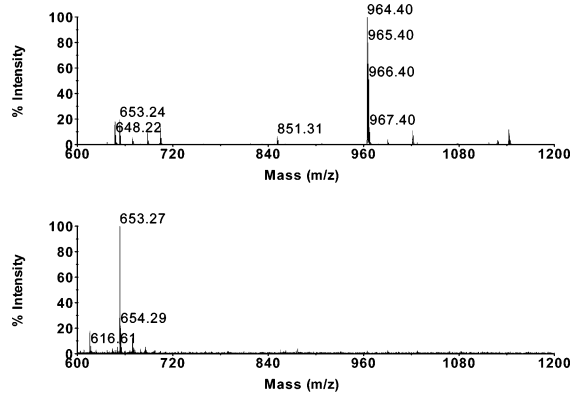

Figure 6. MALDI-MS spectrum characterization of product from light directed synthesis of TMPP−GGFL reveals the desired product to be the major ion at 964.40 Da (964.41 Da theoretical) in the light-exposed region (top) and not in the control region (bottom), which shows a major ion at 653.27 Da corresponding to the sodium adduct of NVOC−GGFL (653.25 Da theoretical).

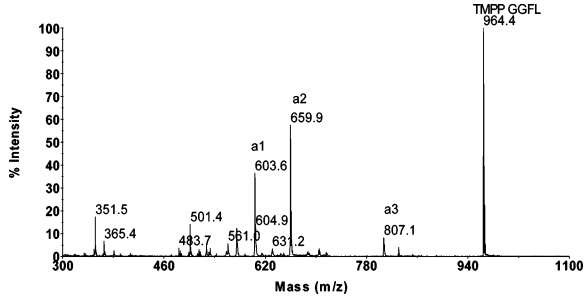

Figure 7. Postsource decay spectra from primary TMPP−GGFL ion allows the sequencing of the peptide via secondary ions a1 = TMPP−G, a2 = TMPP−GG, and a3 = TMPP−GGF.

is observed in the postsource decay spectrum; however, there are several additional "a" ions, which correspond to ions formed from the fragmentation of the amide nitrogen carbon linkage followed by loss of CO. Inspection reveals that these "a" ions correspond to TMPP−GGF, TMPP−GG, and TMPP−G, and the difference in their masses is equivalent to the mass of the missing amino acids.

Conclusion

Porous polymer gel microstructures have been formed using a scanning laser system. It has been shown that large pores can be formed without the use of porogens and that pore formation can be spatially controlled using a focused laser beam. A photolabile protective group has been used to selectively attach fluorescent dye molecules and to make peptides on these microstructures. The high number of peptide attachment sites has also made it possible to use MALDI-MS to determine the peptide mass sequence. This approach opens up many possibilities for constructing complex three-dimensional biomaterials with spatially controlled porous regions and surface functionalization for use in the construction of artificial tissues.

Acknowledgment. We gratefully acknowledge the financial support from the Department of Energy (grant DE-FC36-05GO15016) and NSF (grant DGE-0114434). NSF grant no. CHE-0131222 provided funds to purchase the mass spectrometer. We would also like to thank Sudhir Gudala for development of the scanning software, Saritha Keshammolu for glass slide preparation, and the Center for Solid State Science at Arizona State University for SEM images.

References and Notes

(1) Griffith, L. G.; Naughton, G. *Science* **2002**, *295*, 1009 ff.
(2) Langer, R.; Tirrell, D. A. *Nature (London)* **2004**, *428*, 487−492.
(3) Shieh, S. J.; Vacanti, J. P. *Surgery* **2005**, *137*, 1−7.
(4) Kawata, S.; Sun, H. B.; Tanaka, T.; Takada, K. *Nature (London)* **2001**, *412*, 697−698.
(5) Maruo, S.; Ikuta, K. *Sens. Actuators, A* **2002**, *100*, 70−76.
(6) Maruo, S.; Ikuta, K.; Korogi, H. *Appl. Phys. Lett.* **2003**, *82*, 133−135.
(7) Maruo, S.; Ikuta, K.; Korogi, H. *J. Microelectromech. Sys.* **2003**, *12*, 533−539.
(8) Belfield, K. D.; Schafer, K. J.; Liu, Y. U.; Liu, J.; Ren, X. B.; Van Stryland, E. W. *J. Phys. Org. Chem.* **2000**, *13*, 837−849.
(9) Yu, T. Y.; Ober, C. K. *Biomacromolecules* **2003**, *4*, 1126−1131.
(10) Basu, S.; Cunningham, L. P.; Pins, G. D.; Bush, K. A.; Taboada, R.; Howell, A. R.; Wang, J.; Campagnola, P. J. *Biomacromolecules* **2005**, *6*, 1465−1474.
(11) Bochet, C. G. *J. Chem. Soc., Perkins Trans. 1* **2002**, 125−142.
(12) Pirrung, M. C. *Angew. Chem., Int. Ed.* **2002**, *41*, 1277 ff.
(13) McGall, G. H.; Barone, A. D.; Diggelmann, M.; Fodor, S. P. A.; Gentalen, E.; Ngo, N. *J. Am. Chem. Soc.* **1997**, *119*, 5081−5090.
(14) Fodor, S. P. A.; Read, J. L.; Pirrung, M. C.; Stryer, L.; Lu, A. T.; Solas, D. *Science* **1991**, *251*, 767−773.
(15) Svec, F.; Frechet, J. M. J. *Anal. Chem.* **1992**, *64*, 820−822.
(16) Svec, F.; Frechet, J. M. J. *Science* **1996**, *273*, 205−211.
(17) Svec, F.; Peters, E. C.; Sykora, D.; Frechet, J. M. J. *J. Chromatogr., A* **2000**, *887*, 3−29.
(18) Rosenberg, J. E.; Flodin, P. *Macromolecules* **1987**, *20*, 1518−1522.
(19) Rosenberg, J. E.; Flodin, P. *Macromolecules* **1987**, *20*, 1522−1526.
(20) Flodin, P.; Rosenberg, J. E. *Biol. Chem. Hoppe-Seyler* **1987**, *368*, 743−743.
(21) Yu, C.; Davey, M. H.; Svec, F.; Frechet, J. M. J. *Anal.Chem* **2001**, *73*, 5088−5096.
(22) Yu, C.; Xu, M. C.; Svec, F.; Frechet, J. M. J. *J. Polym. Sci., Part A: Polym. Chem.* **2002**, *40*, 755−769.
(23) Rohr, T.; Hilder, E. F.; Donovan, J. J.; Svec, F.; Frechet, J. M. J. *Macromolecules* **2003**, *36*, 1677−1684.
(24) Luo, Y.; Shoichet, M. S. *Nat. Mater.* **2004**, *3*, 249−253.
(25) Luo, Y.; Shoichet, M. S. *Biomacromolecules* **2004**, *5*, 2315−2323.
(26) Northen, T. R.; Woodbury, N. W. *Langmuir* **2005**, *21*, 4949−4953.
(27) Huang, Z. H.; Wu, J.; Roth, K. D. W.; Yang, Y.; Gage, D. A.; Watson, J. T. *Anal. Chem.* **1997**, *69*, 137−144.
(28) Chiellini, F.; Bizzarri, R.; Ober, C. K.; Schmaljiohann, D.; Yu, T. Y.; Saltzman, W. M.; Solaro, R.; Chiellini, E. *Macromol. Symp.* **2003**, *197*, 369−379.
(29) Barton, A. F. M. *CRC Handbook of Solubility Parameters and Other Cohesion Parameters*, 2nd ed.; CRC Press: Boca Raton, 1991.
(30) Horak, D.; Dvorak, P.; Hampl, A.; Slouf, M. *J. Appl. Polym. Sci.* **2003**, *87*, 425−432.

BM0506952